INVESTIGATION AND SUPPRESSION OF HIGH DYNAMIC RESPONSE ENCOUNTERED ON AN ELASTIC SUPERCRITICAL WING

David A. Seidel, William M. Adams, Jr.,
Clinton V. Eckstrom, and Maynard C. Sandford
NASA Langley Research Center
Hampton, Virginia

BACKGROUND

The elastic semispan wing used in the present study is from the NASA program Drones for Aerodynamic and Structural Testing (DAST) and is the right wing panel from the second Aeroelastic Research Wing (ARW-2). The DAST ARW-2 wing was designed to flutter within the flight envelope of the drone aircraft to which it was to be attached. The wing had an aspect ratio of 10.3, a leading-edge sweep angle of 28.8°, and a supercritical airfoil. The wing was designed for a cruise condition of M = 0.80, C_L = 0.53 (α = 1.3°), and an altitude of 46,800 feet (q = 127 psf). The wing had three hydraulically driven trailing-edge control surfaces and was instrumented with dynamic pressure transducers and accelerometers.

An unusual transonic instability was encountered near M = 0.9 during an unsteady pressure test of the DAST ARW-2 wing in October 1983 in the Langley Transonic Dynamics Tunnel (TDT). This unusual transonic instability boundary was predicted using a subcritical response technique. This instability was predicted to occur at an almost constant Mach number of 0.9 for all dynamic pressures tested. The wing motion was primarily first wing bending mode response and was angle of attack dependent. Single degree-of-freedom bending mode oscillations have also been encountered during experiments with several other aircraft configurations. These oscillations have been observed on a low aspect ratio wing with subsonic airfoil shape, on the B-1A during a wind-up turn, on the canard of the HIMAT aeroelastic model at negative angle of attack, and on a forward swept wing force model panel at a negative angle of attack. Linear theory flutter analysis was unable to predict any of these oscillations. (Fig. 1.)

- DAST ARW-2 Wing
  - Aeroelastic wing designed to flutter in flight envelope
  - High-aspect-ratio supercritical wing
  - Design cruise Mach number = 0.8
  - Wing heavily instrumented for unsteady pressure data acquisition
- Wing tested in TDT, October 1983 (AIAA 85-0598-CP)
  - Instability unexpectedly encountered
    - Boundary predicted using subcritical response technique
    - Motion predominantly 1st wing bending
    - Boundary at almost constant Mach number of 0.90
    - Angle-of-attack sensitive
  - Similar phenomena observed for other aircraft

Figure 1

DAST ARW-2 WING IN TDT

Figure 2 shows the wing and fuselage configuration mounted in the wind tunnel. The elastic semispan wing used in the present study is the DAST ARW-2 right wing panel. A half-body fuselage was used to simulate the drone fuselage. This fuselage had shorter nose and tail sections than does the drone fuselage since no supersonic tests were to be made. The center section of the fuselage was similar to the actual drone fuselage in both diameter and wing location to generate the proper airflow over the inboard section of the wing. Both the fuselage and the wing were mounted on a remotely controlled turntable mechanism located on the tunnel sidewall.

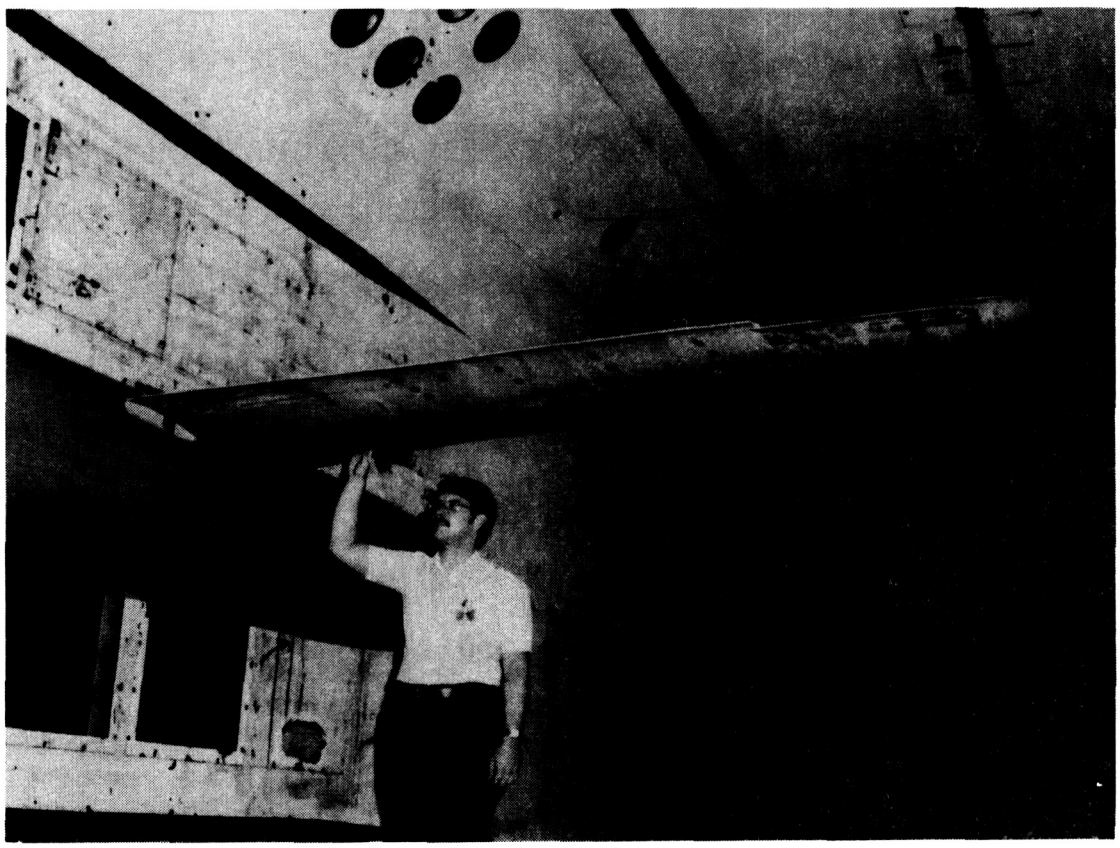

Figure 2

DAST ARW-2 WING

The wing planform is shown in figure 3. The wing had an aspect ratio of 10.3 with a leading-edge sweep angle of 28.8°. The wing was equipped with three hydraulically driven control surfaces, two inboard and one outboard. For this test, the inboard surfaces were held fixed at 0° deflection and only the outboard surface was deflected statically. The outboard surface hinge line was located at 77 percent of local chord.

Also shown in figure 3 are the locations of the wing instrumentation. The instrumentation consisted of 191 dynamic pressure transducers and 10 accelerometers. In addition, strain gauge bridges were located near the wing root to measure bending moments. Small potentiometers were used to measure the control surface angular displacement. The model angle of attack was measured by a servo accelerometer that was mounted near the wing root. Both steady and unsteady pressures were obtained using differential pressure transducers referenced to the tunnel's static pressure. Streamwise rows of upper and lower surface pressure orifices were located at six span stations: η = 0.274, 0.476, 0.599, 0.707, 0.871 and 0.972. The fifth row at η = 0.871 lies along the mid-span of the outboard control surface. All of these surface orifices were connected to pressure transducers by matched tubes having an inner diameter of 0.040 inch and a length of 18 inches. In order to determine the tube transfer functions needed to correct the unsteady pressure data from these matched-tube transducers, simultaneous measurements were also obtained from a row of in situ transducers mounted on the wing upper surface at η = 0.875, parallel to the fifth row of surface orifices. Dynamic wing deflections were determined using the 10 accelerometers.

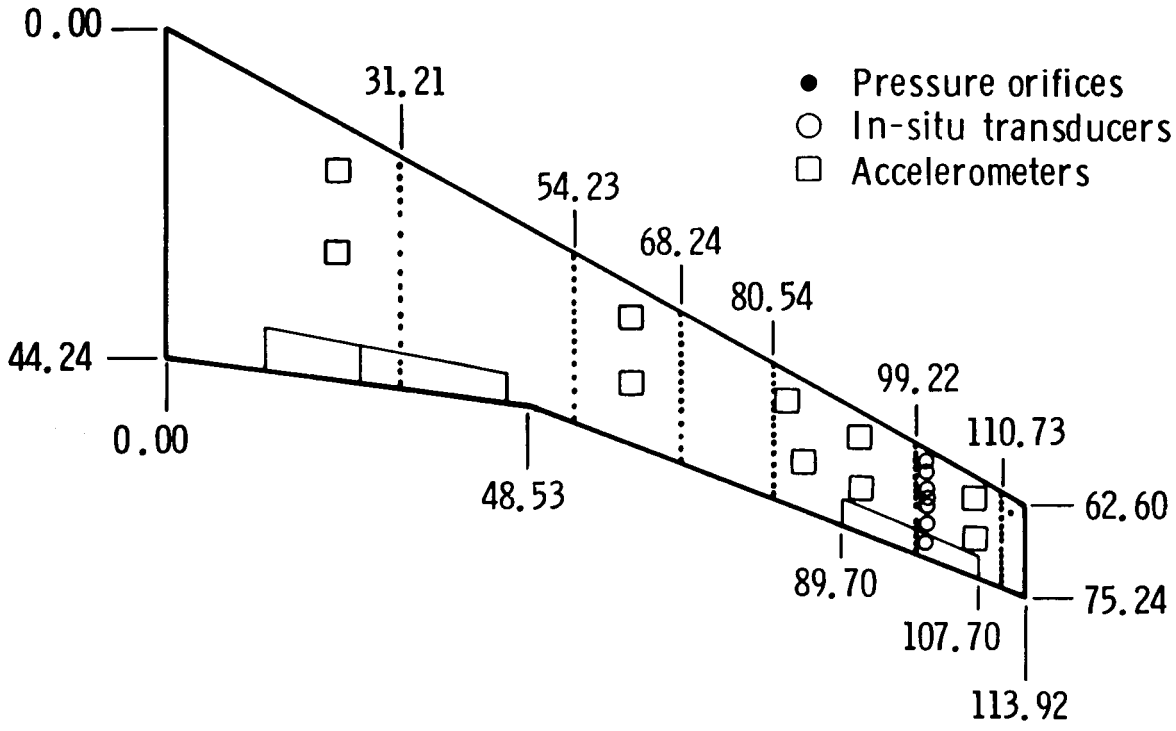

Figure 3

INSTABILITY BOUNDARY PREDICTED DURING FIRST TEST

During the first test of the ARW-2 wing in the TDT an unusual wing instability, with motion similar to the wing first bending mode, was encountered. The boundary was determined for a wing angle of attack and control surface deflection of 0° as shown in figure 4. Also shown in figure 4 as a solid line is the predicted linear theory (doublet lattice theory) flutter boundary, which is of a conventional nature. The measured boundary was determined using a familiar subcritical response technique known as peak-hold. The boundary was predicted to occur at a nearly constant Mach number of 0.90 beginning at a low dynamic pressure of about 50 pounds per square foot (psf) (R = 874,000) and rising nearly vertical to over 300 psf (R = 5,300,000). The observed wing motion during the instability was similar to the wing first bending mode, the frequency of which was 8.3 Hz wind-off. The instability frequency was 8.6 Hz at the lowest dynamic pressure and increased to about 13 Hz at the highest dynamic pressure.

Because of recent interest in angle-of-attack effects and shock induced effects on wing instabilities, several additional test runs were made. These runs include variation of the wing angle of attack, comparison using air or Freon as the test medium and comparison with and without a transition strip near the wing leading edge. The instability was found to be sensitive to variation in angle of attack and, generally, the minimum damping occurred at or near zero wing root angle of attack. In figure 4 the solid symbol indicates the Mach number and dynamic pressure where the comparison tests were made. The results showed no significant difference in the instability boundary for tests in air or Freon. Reynolds number values in Freon are approximately 3.1 times greater than those obtained in air. There were also no significant differences for tests in Freon with or without a transition strip.

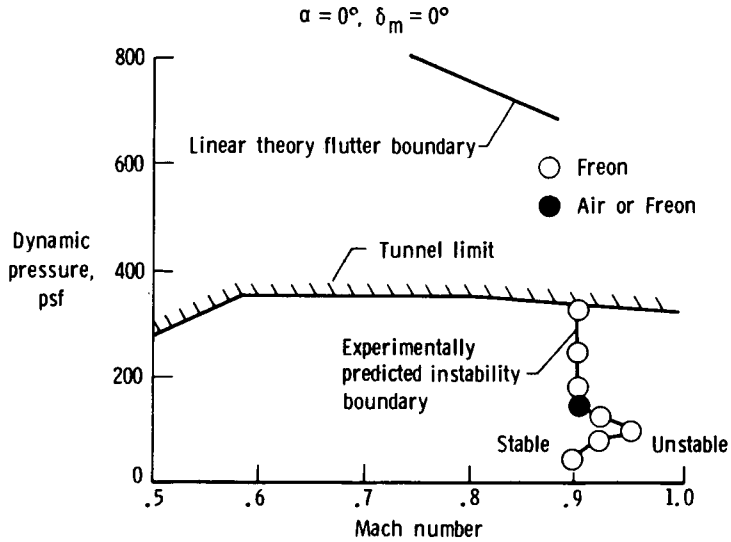

Figure 4

DAST ARW-2 WING RETEST

A second wing tunnel test was performed on the DAST ARW-2 wing to further investigate the unusual instability. The primary purpose of the test was to establish firmly the existence of the instability boundary and to gather wing response data and dynamic pressure measurements to help understand the mechanism forcing the wing oscillations. A secondary purpose was to design an active control system to suppress the wing response using the outboard control surface.

Dynamic pressures and wing deflections were measured for a large number of test conditions in the TDT using Freon as a test medium. Data were taken at Mach numbers from 0.5 to 0.96 for two stagnation pressures. For a Mach number range of 0.8 - 0.96 the two stagnation pressures gave a dynamic pressure variation of 125 - 166 pounds per square foot (psf) and 260 - 340 psf. These two stagnation pressures will be referred to as the low and high density conditions.

Wool tufts were used to visualize the flow patterns on the wing in the instability region. Static wing tip deflection was measured over the range of test conditions. The effect on dynamic wing response of wing angle of attack, static outboard control surface deflection and a spanwise fence on the lower surface were investigated. All dynamic wing response data presented is obtained from the rear wing tip accelerometer. (Fig. 5.)

- Purpose
  - Obtain further information on mechanism of non-classical instability
    - Acquire experimental database
  - Assess feasibility of active suppression of wing response (AIAA 87-0881-CP)
- Method
  - Probe instability region
  - Record unsteady pressure and wing acceleration
  - Flow visualization
  - Measure wing deflection

Figure 5

WING-TIP ACCELEROMETER PEAK-HOLD RESPONSE - MACH EFFECTS

Figure 6 shows the peak-hold results from the wing tip accelerometer for both the low and high density conditions. The wing angle of attack and control surface deflection were held at 0°. The data show that no instability was found but instead a region of high dynamic wing response was observed. For the lower density condition (q = 125 - 166 psf) the wing motion reaches a maximum at M = 0.93 and then rapidly decreases with increasing Mach number. The same trend occurs for the higher density condition (q = 260 - 340 psf) with maximum wing motion occurring near M = 0.92. The observed wing tip maximum dynamic amplitudes are noted in figure 6. At the lower density condition, the amplitude of the wing tip motion was approximately 2 inches peak-to-peak. At the higher density condition, which has double the dynamic pressure, the amplitude of the wing tip motion doubled to approximately 4 inches peak-to-peak.

Also shown in figure 6 at the higher density condition and M = 0.92 is a single point for $\alpha = -1°$ where 6 inches peak-to-peak amplitude of wing tip motion was observed. At this condition the wing motion was so severe that the tunnel bypass valves were opened to rapidly reduce the dynamic pressure and associated wing motion.

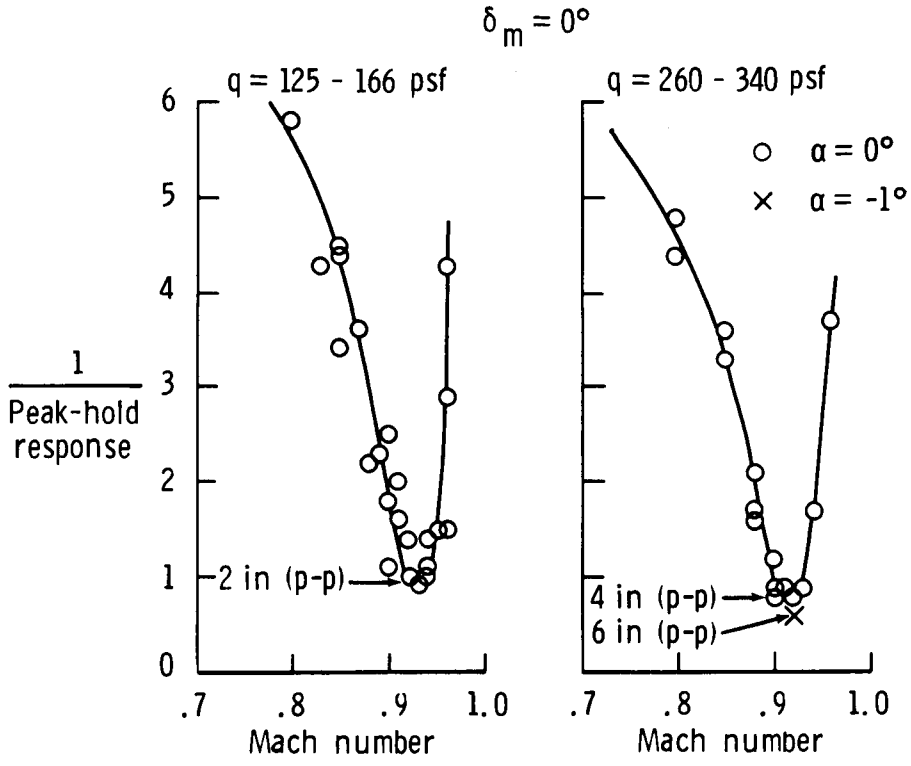

Figure 6

WING-TIP ACCELEROMETER PEAK-HOLD RESPONSE - ANGLE OF ATTACK EFFECTS

Figure 7 shows the peak-hold results from the wing tip accelerometer for three wing angles of attack at the lower density condition. The mean control surface deflection was held at 0°. As shown in the figure, the maximum dynamic wing response occurred for a wing angle of attack of 0° at M = 0.93. Changing the wing angle of attack to 2 and -2 degrees decreased the maximum wing response and shifted the corresponding Mach number to 0.94. Similar angle of attack trend results were seen at the higher density condition. Data were taken for wing angles of attack of 1, 0 and -1 degrees up to M = 0.9 and fell within the scatter of the experimental data observed at 0° as shown in figure 6. Therefore it is believed that for this configuration the maximum wing response occurs when the wing angle of attack is nominally at 0°.

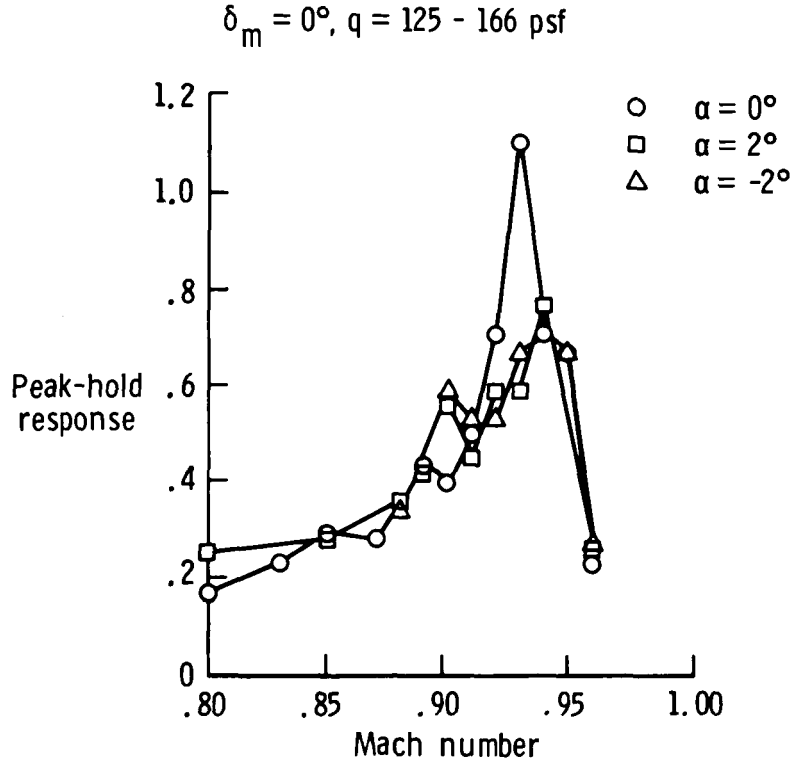

Figure 7

WING-TIP ACCELEROMETER PEAK-HOLD RESPONSE - OUTBOARD CONTROL EFFECTS

Figure 8 shows the peak-hold results from the wing tip accelerometer for three outboard control surface mean deflection angles at the lower density condition. The wing angle of attack was set at 0°. The figure shows a small increase in wing response for the control surface deflection of 6° (trailing-edge down). However, a significant reduction in wing response is shown for a deflection of -6°. The wing tip maximum response peak is reduced by half and shifted to a lower Mach number of 0.91.

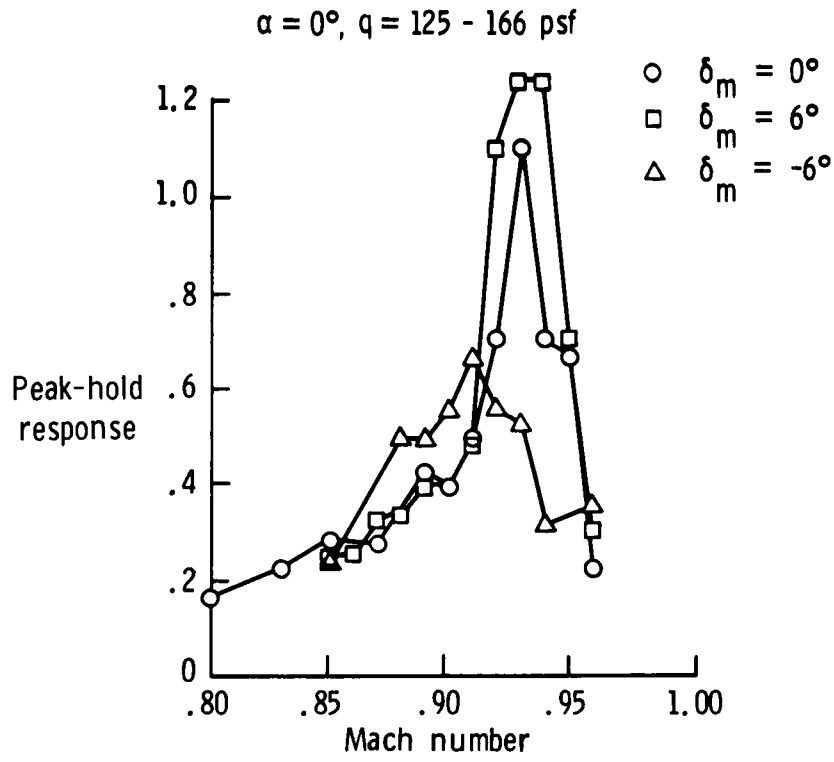

Figure 8

DAST ARW-2 WING WITH LOWER SURFACE SPANWISE FENCE

In an attempt to disturb the flow and change the dynamic wing response, a 1/2-inch high spanwise fence was attached to the lower surface at approximately the 60% local chordline as shown in figure 9. The fence ran from the wing planform break (η = 0.426) to within 5 inches of the wing tip (η = 0.956). The fence was made up of 5 separate one foot-long pieces of aluminum placed end to end to minimize increasing the wing stiffness.

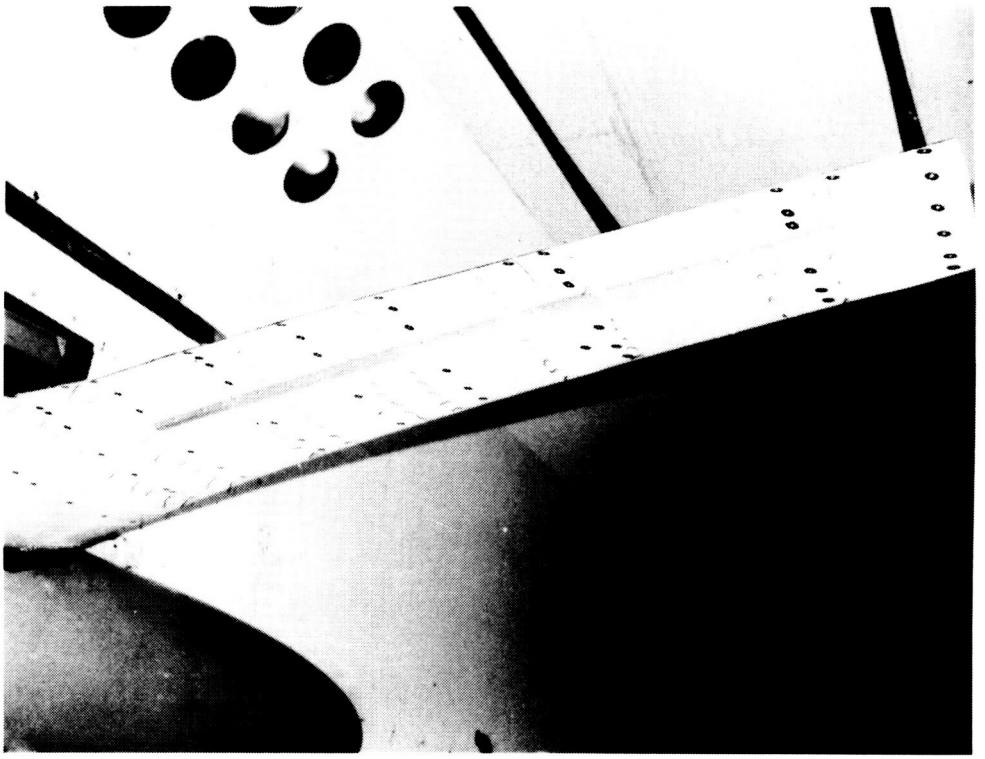

Figure 9

WING-TIP ACCELEROMETER PEAK-HOLD RESPONSE - SPANWISE FENCE EFFECTS

The effect of the fence on the wing tip accelerometer peak-hold response at the lower density condition is shown in figure 10. The fence has a significant effect upon the wing response, lowering the amplitude of maximum wing motion and shifting the peak value to a lower Mach number of 0.90.

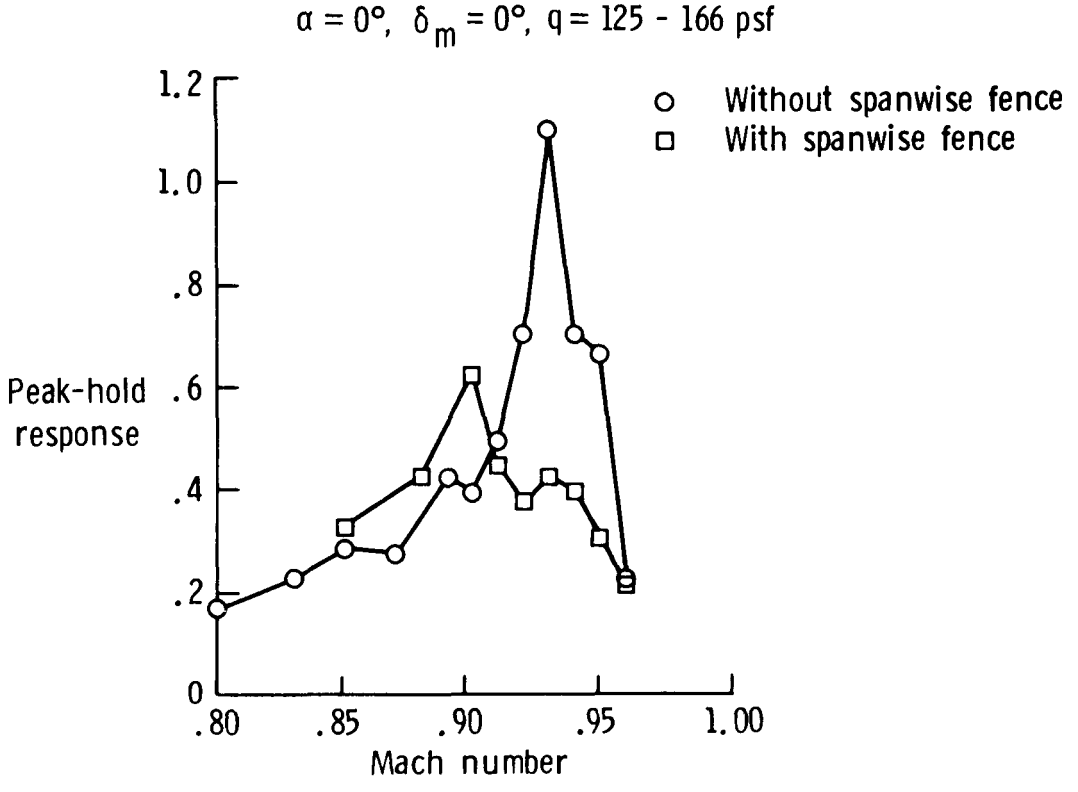

Figure 10

DAST ARW-2 WING WITH WOOL TUFTS

Wool tufts were placed on the upper and lower wing surfaces for several test runs to visualize the flow patterns on the wing. The tufts were placed on eight span stations located at η = .517, .558, .635, .671, .761, .816, .905 and .938, as shown in figure 11. The tufts were one inch long and on the six inboard span stations were located at ever 10% of local chord. On the two outboard span stations the tufts were located between 10 and 90% chord at every 20% of local chord.

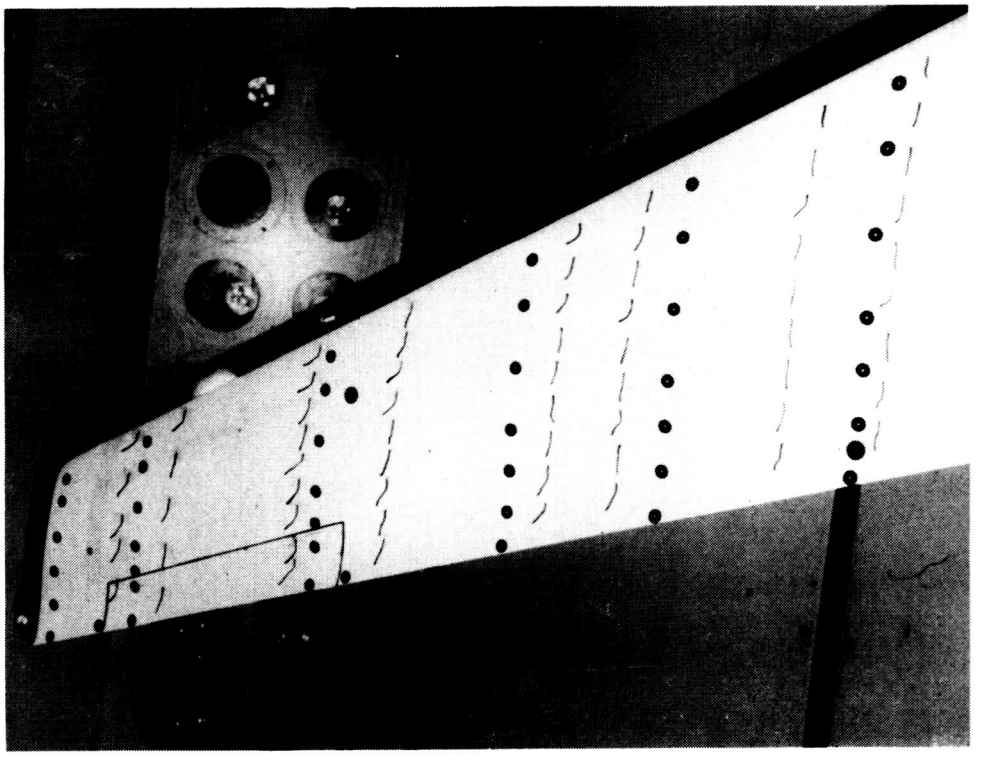

Figure 11

ORIGINAL PAGE
BLACK AND WHITE PHOTOGRAPH

SEPARATED FLOW REGIONS INDICATED BY WOOL TUFTS

Figure 12 lists the regions of separated flow on the wing as indicated by the tuft data for Mach numbers from 0.85 to 0.96 at the lower density condition. Upper surface flow separation is first indicated at M = 0.88. The region of separated flow expands upstream and outboard as Mach number increases to 0.94 and then remains constant to M = 0.96. Flow separation on the lower surface is initially indicated at M = 0.90. The region of separated flow expands upstream and outboard as Mach number increases of 0.94. At M = 0.96 the region of separated flow on the lower surface decreases, moving downstream and inboard.

	Region of separated flow			
	Upper surface		Lower surface	
M	x/c	η	x/c	η
.85	----	----	----	----
.88	.8 - 1.0	.517 - .816	----	----
.90	.7 - 1.0	.517 - .905	.6 - 1.0	.635 - .761
.92	.7 - 1.0	.517 - .938	.6 - 1.0	.635 - .938
.94	.6 - 1.0	.517 - .938	.5 - 1.0	.635 - .938
.96	.6 - 1.0	.517 - .938	.6 - 1.0	.635 - .905

Figure 12

MEAN PRESSURE DISTRIBUTIONS

Figure 13 shows the mean chordwise pressure distribution at the 87.1% span station for nine Mach numbers at the lower density condition. The wing angle of attack and outboard mean control surface deflection were 0°. As Mach number increases, a shock develops on the upper surface at M = 0.85 and becomes quite strong at M = 0.89. The criteria used to determine trailing-edge flow separation from mean pressure measurements is the attainment of negative pressure coefficients at the 95% chord location. When negative pressures are sustained aft of this location, the flow is considered to be separated. Based upon the mean pressure distributions shown in figure 13, it appears that flow separation on the upper surface is evident at M = 0.92 and is established strongly at M = 0.94. The lower surface develops a strong shock at M = 0.92 and the pressure distributions indicate flow separation at M = 0.96.

Comparing these data to the separated flow regions indicated by wool tufts shown in figure 12 leads to two conclusions. The first is that the mean pressure data give an incomplete picture of the flow separation. The mean pressure data, taken at η = 0.871, does not indicate flow separation on the upper surface until M = 0.92 while the wool tufts indicate separation in the region of the pressure transducers near M = 0.89. Flow separation on the lower surface is not indicated by the mean pressures until M = 0.96 while the tufts indicate separation in the region at M = 0.92. The second conclusion is that flow separation, as shown by the tuft data, coincides with the occurrence of strong shocks on a surface, as shown by the mean pressure data in figure 13. This flow separation occurs near M = 0.89 on the upper surface and M = 0.92 on the lower surface at the 87.1% span station.

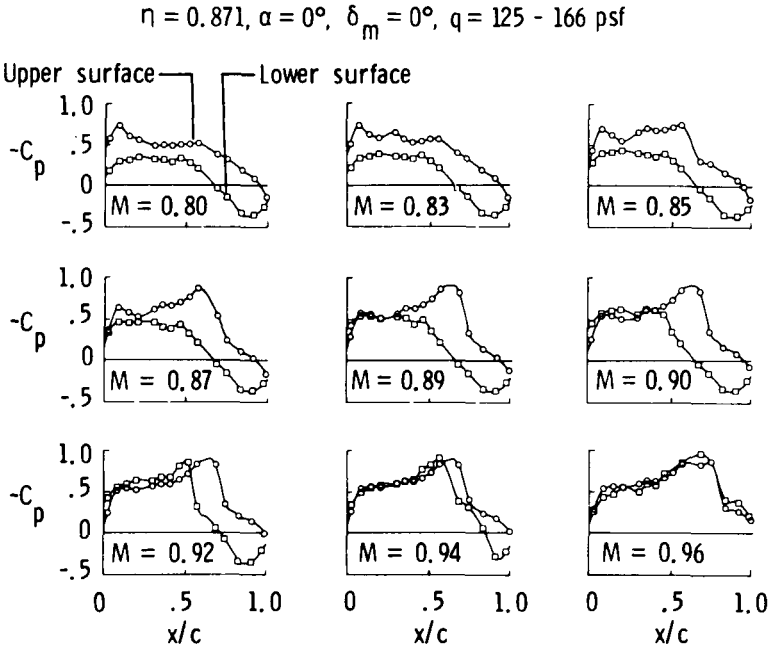

Figure 13

STATIC WING TIP DEFLECTIONS

During the test, measurements of the mean wing tip deflection and twist were made using an optical cathetometer instrument focused on a straight line drawn on the outboard tip of the wing. The results of the wing tip measurements for the lower density condition at a wing angle of attack and mean control surface deflection of 0° are shown in figure 14. The wing tip deflection and twist increase as Mach number increases up to a maximum near M = 0.85. At higher Mach numbers the wing tip deflection and twist values decrease rapidly as the Mach number increases. This agrees with the tuft data which show flow separation beginning on the upper surface at M = 0.88, causing loss of lift (see figure 13) and the resulting decrease in wing deflection and twist.

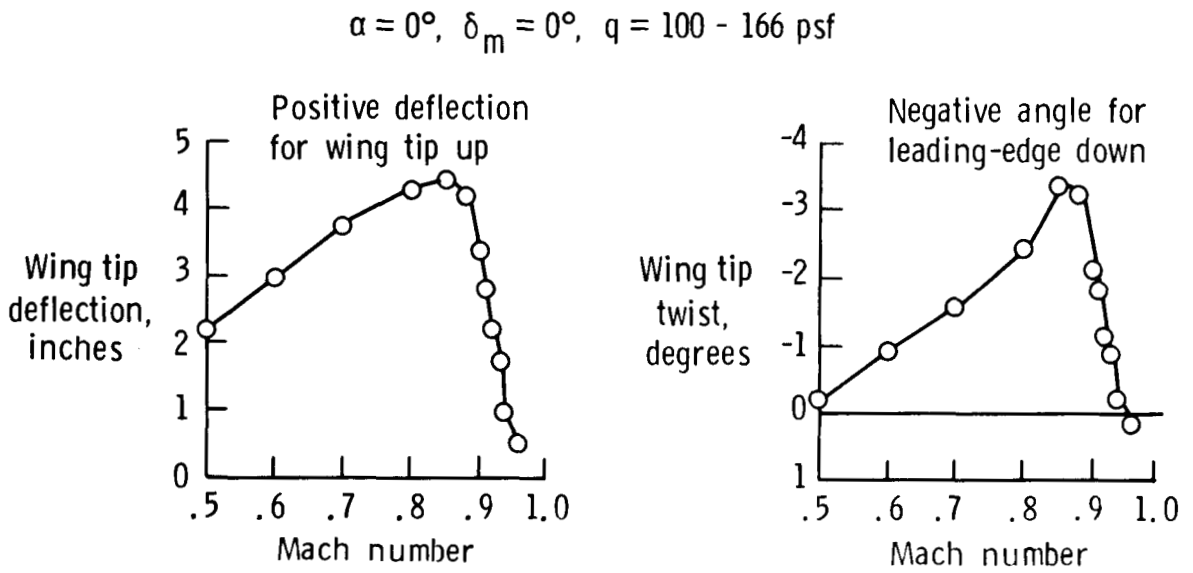

Figure 14

INSTANTANEOUS PRESSURE DISTRIBUTIONS

Figure 15 shows the instantaneous chordwise pressure distribution at the 87.1% span station for M = 0.92, α = -1° and δ_m = 0°. This is the condition at which 6 inch peak-to-peak wing tip motion occurred (figure 6). The instantaneous pressure distributions are shown for the maximum and minimum vertical wing tip deflection. Based upon the pressure at 95% chord, at the maximum wing tip deflection the flow aft of the shock is separated on the upper and lower surfaces. The flow is attached on both surfaces when the vertical tip deflection is a minimum.

This figure points out an important feature of this dynamic motion. At conditions where large amplitude dynamic motion is encountered, the trailing-edge flow begins a pattern of separating and reattaching on the wing, which coincides with the shock wave motion. As the Mach number is increased above 0.92 the flow behind the shock remains separated (see figure 13) and the amplitude of the motion rapidly decreases (see figure 6). Thus it appears that the dynamic wing response is related to chordwise shock motion in conjunction with shock induced flow separation and reattachment on both the upper and lower surfaces. This conclusion is supported further by the results obtained when the spanwise fence was attached to the wing lower surface. The fence prevented reattachment of the flow on that surface and the maximum wing motion was found to be dramatically reduced as shown in figure 10.

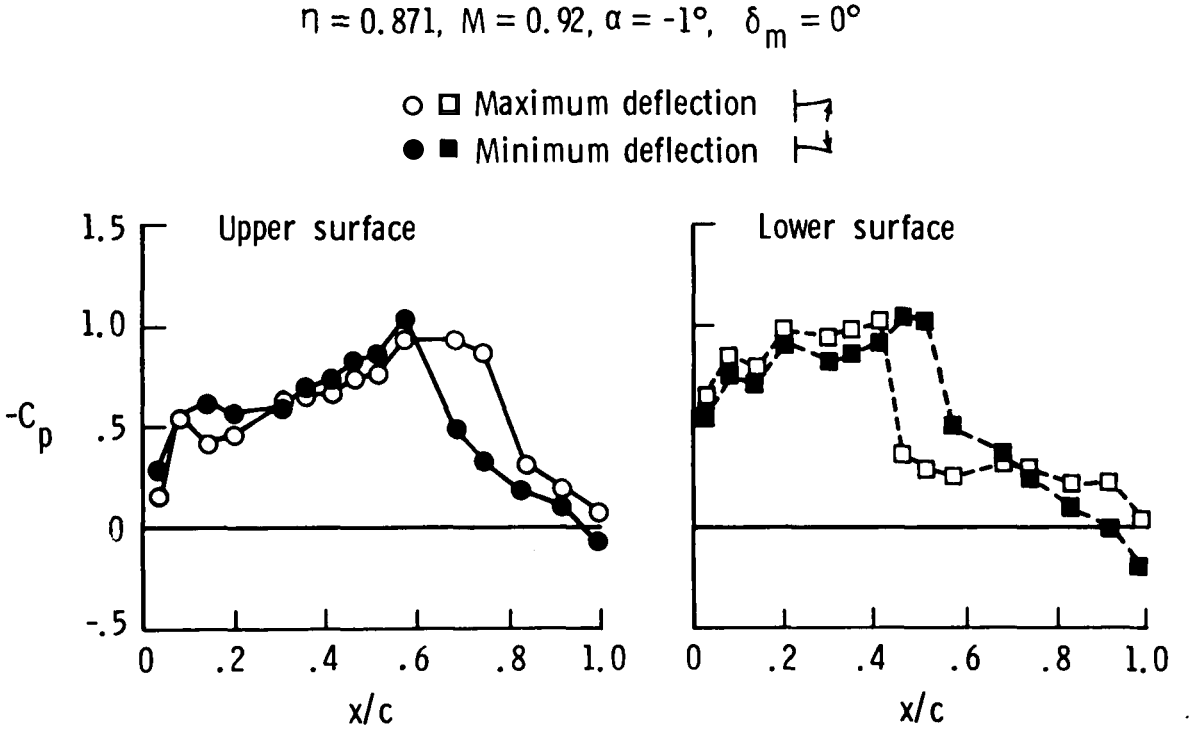

Figure 15

C-3

PRESSURE VARIATION WITH TIME

Figure 16 shows a time history of upper and lower surface pressures at the same span station and flow conditions as given in figure 15. All pressures are arbitrarily plotted so that they fit near each other. However, the last chordwise pressures on both surfaces are plotted with a zero reference line. For the last chordwise pressures, the figure clearly shows the separation and reattachment of flow in the trailing-edge region of both surfaces as the pressure values fluctuate above and below zero. The shock motion, as indicated by large pressure variations, is also shown in the figure. For example, the upper surface shock can be seen to move from in front of 68.0% of local chord to behind 74.2%. The lower surface shock moves from in front of 46.0% to behind 51.3%. At the bottom of the figure the measured wing root bending moment time history is plotted for reference. For the observed motion, the wing root bending moment is proportional to wing tip displacement, bending maximum for maximum positive (up) wing tip position.

The alternating separation and reattachment of the flow on the upper and lower surfaces explains the discrepancy between the mean pressure and wool tuft data. The mean pressure data give an average of the pressure values in the trailing-edge region. If, on the average, the flow is attached most of the time, the mean pressure distributions will indicate that the flow is attached. The mean data give an accurate indication of separation only when the flow remains separated most of the time. Another point to note is that while the wool tufts indicate flow separation, they are inadequate for indicating the subsequent flow reattachment.

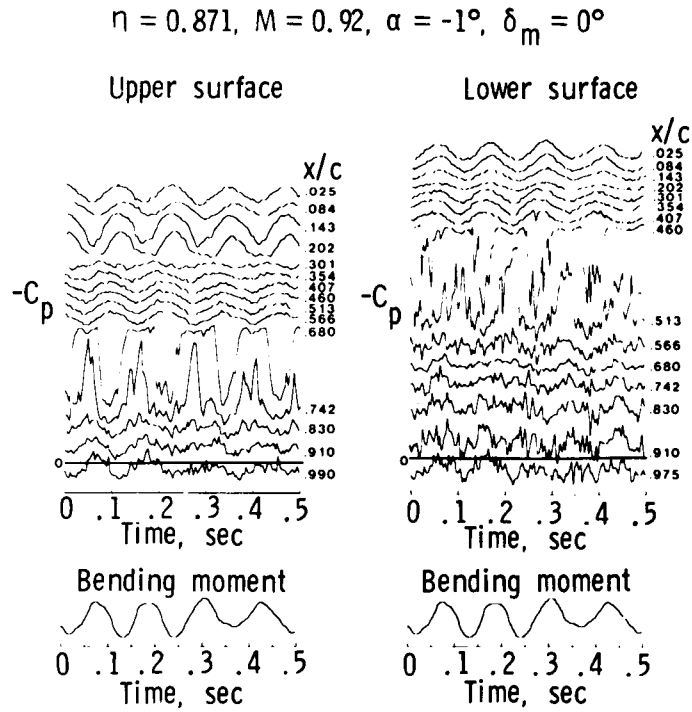

Figure 16

DEMONSTRATION OF ACTIVE SUPPRESSION OF WING RESPONSE

The design of a controller to actively suppress the wing response presented several challenges. Flutter analysis based upon linear potential flow aerodynamic theories did not predict the wing response. The approach adopted was to develop approximate linear models by utilizing forced response data taken during the previous tunnel entry in October 1983. Key transfer functions were estimated from the forced response data for a range of test points as the region of dynamic wing response were approached. Because of the uncertain nature of the transfer function estimates upon which the control law was based, additional transfer function and controller performance data were gathered during the test and used to modify the controller to obtain satisfactory performance. Computer algorithms were written to give near real-time assessment of controller performance.

During the test several sets of fast sine sweep data were taken and averaged for improved transfer function estimation. The loop transfer function was estimated using Fast Fourier Transform (FFT) techniques and, with the feedback loop open, provided a near real-time assessment of controller performance. The controller was modified as necessary and the control loop closed. Fast sine sweep data were again taken to evaluate controller performance. (Fig. 17.)

- Challenges
  - Mathematical models more uncertain than normal
  - Requirement to estimate key transfer functions from experimental data
  - Development/assembly of algorithms that allow near real-time assessment of controller performance during test
- Method
  - Upgrade transfer function estimates
  - Evaluate controller performance with loop open
  - Confirm modified controller performance by closing loop

Figure 17

CLOSED LOOP BLOCK DIAGRAM

The inability of flutter analyses based upon linear potential flow aerodynamic theories to predict the apparent instability led to a decision to attempt to design a control law based upon forced response data from the previous TDT entry (October 1983). Figure 18 depicts the block diagram for the closed-loop single-input/single-output system. The transfer function estimates, $\hat{\ddot{z}}/\delta_a$, were obtained from response data due to fast sine sweep inputs into the aileron actuator, G_A. These data were available for a number of test points in the range of Mach number $0.7 < M < 0.85$. Unfortunately, the accuracy of the estimates became more suspect as the apparent stability boundary, where good estimates were most needed, was approached. Nevertheless, these transfer function estimates were employed in the preliminary design of a control law, H, to add damping to the critical mode.

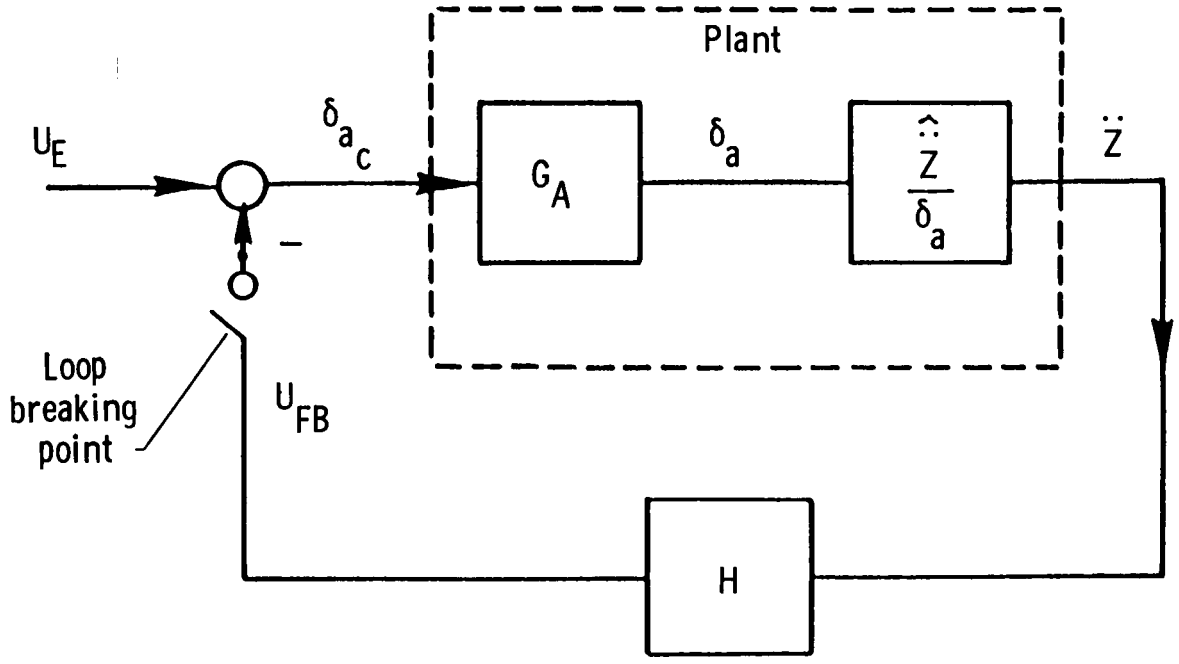

Figure 18

ROBUSTNESS MAXIMIZATION

The objective of the control law design activity was to add damping in the critical frequency range without degrading the stability characteristics of the higher frequency modes. The approach taken was to define, for a range of test points, the compensation, H(s), required to modify the amplitude and phase of the accelerometer outputs such that damping was added in a frequency band centered at the frequency of the first elastic mode. The control law form chosen is shown in figure 19.

T(s) is a fixed low pass filter chosen to attenuate the feedback control so that higher frequency elastic modes were not affected. The factor adjacent to T(s) concentrates the control effort in the frequency region, ω_1, of the first elastic mode; the frequency, $\omega_1(M,q)$, depended upon Mach number, M, and dynamic pressure q. The parameter ζ was fixed at 0.2. The choice, ζ=0.2, was made to confine the control activity in a narrow band around ω_1. In retrospect, a larger value of ζ would probably have resulted in more attenuation of the response due to turbulence and could have been used safely since the frequency of the second elastic mode was about 32 Hz. The remaining part of H(s) factor has variable coefficients $\{D_i(M,q),\ i=1,5\}$ which were used as control design variables to allow proper amplitude and phasing for robustness.

Values for the variable parameters were found for each test point such that the minimum singular value of the return difference transfer function was maximized subject to gain and phase margin constraints. The search for the optimizing set $\{D_i^*(M,q)\}$ was done using a nongradient constrained optimization approach.

Find values for the design variables D_i where

$$H = D_1 \underbrace{\frac{(S^2 + D_2 S + D_3)}{(S^2 + D_4 S + D_5)}}_{\text{Phasing adjustment}} \underbrace{\frac{2\zeta\,\omega_1 S}{S^2 + 2\zeta\,\omega_1 S + \omega_1^2}}_{T(S)}$$

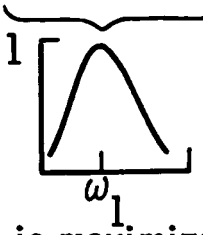

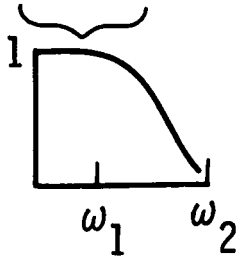

Such that

- Minimum singular value is maximized
- Good gain and phase margins

Figure 19

ACCELEROMETER PEAK-HOLD RESPONSE

Closed-loop performance is shown in figure 20 in terms of frequency domain peak-hold responses. Peak-hold is a subcritical response technique used in predicting flutter boundaries wherein the autospectrum of an output is obtained for a block of data. Subsequent autospectra are taken for a number of blocks of data and the peak value at each frequency out of the entire set of blocks is retained (held). As the point of neutral stability of a mode is approached, the amplitude at its resonant frequency approaches infinity. Thus, by observing the variation in the peaks held, or typically, their reciprocals, as a function of test condition changes, one obtains an indication of changes in damping ratio and a prediction of where an instability might occur.

The figure shows peak-hold responses with the control system loop open and closed both for turbulence only and turbulence plus fast sine sweep excitation. It is seen that the controlled cases have lower responses than the uncontrolled cases over the entire Mach number range. The controlled response is sharply attenuated at the first elastic mode resonant frequency and somewhat amplified on either side of it as compared with the uncontrolled case. The amplification at the slightly higher frequency is due to a lightly damped mode introduced by the controller. Increasing the controller badwidth by selection of a lager value for ζ, as mentioned earlier, would probably have allowed further reduction in the controlled response. Control effort due to turbulence excitation varied from a peak feedback signal magnitude of approximately 0.25° at M = 0.70 to 2.3° at M = 0.92 for these cases.

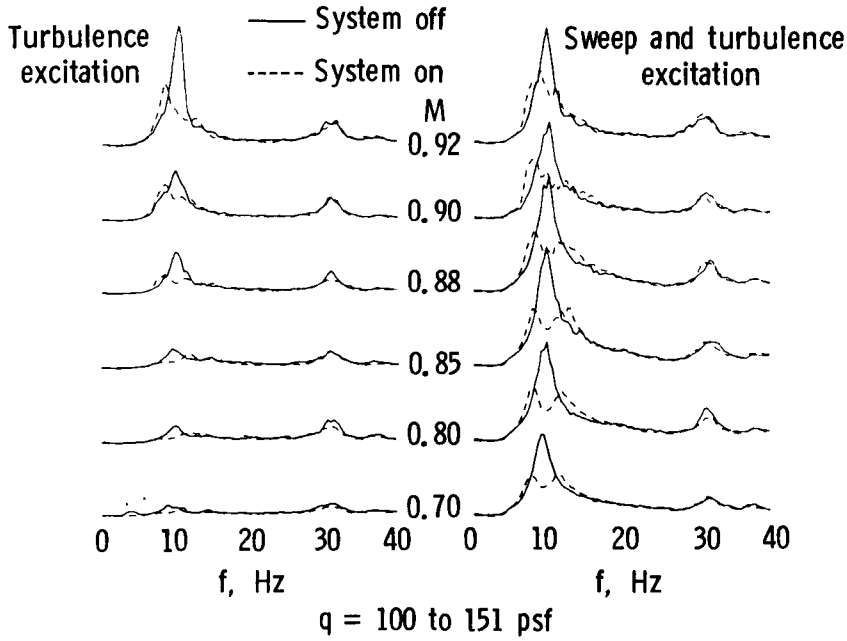

Figure 20

CONCLUDING REMARKS

The DAST ARW-2 wing had been tested previously in the NASA Langley TDT and an unusual instability boundary was predicted based upon subcritical response data. Contrary to the predictions, no instability was found during the present test. Instead a region of high dynamic wing response was observed which reached a maximum value between Mach numbers 0.92 and 0.93. The amplitude of the dynamic response increased directly with dynamic pressure.

The response appears to be related to chordwise shock movement in conjunction with flow separation and reattachment on the upper and lower wing surfaces. The onset of flow separation coincided with the occurrence of strong shocks on a surface. Instantaneous pressure distributions indicated that the flow was intermittently separating and reattaching near the trailing edge under conditions of maximum wing motion. The dynamic wing response was sensitive to angle of attack, with maximum motion occurring near $\alpha = 0°$. Static deflection of the outboard control surface significantly decreased the dynamic response for $\delta m = -6°$. A spanwise fence installed on the lower surface to disturb the flow pattern resulted in a significant decrease in dynamic wing response.

A controller was designed to suppress the wing response. The control law attenuated the response as compared with the uncontrolled case and added a small but significant amount of damping from M = 0.70 to M = 0.92 for the lower density condition (q = 100 - 151 psf).

The unsteady pressure and response data acquired during this test constitute a valuable data base to be used for further study of this unusual phenomena and for validation of unsteady CFD codes. (Fig. 21.)

- No "hard flutter" point obtained although amplitude increases as dynamic pressure increases
- Response coincides with onset of shock-induced separation and reattachment
- Response affected by angle-of-attack, outboard control surface position, and a spanwise fence on the lower surface
- Active suppression successfully demonstrated, significant damping added with feedback loop closed
- Unsteady pressure data acquired during dynamic response for further analysis and use in code validation work

Figure 21